ORNL/TM-12831

ornl

OAK RIDGE
NATIONAL
LABORATORY

MARTIN MARIETTA

Neutron Dosimetry of the HFIR Hydraulic Facility

S. T. Mahmood
S. Mirzadeh
K. Farrell
J. V. Pace III
B. M. Oliver

MANAGED BY
MARTIN MARIETTA ENERGY SYSTEMS, INC.
FOR THE UNITED STATES
DEPARTMENT OF ENERGY

ORNL/TM-12831

Neutron Dosimetry of the HFIR Hydraulic Facility

S. T. Mahmood, S. Mirzadeh, K. Farrell,
J. V. Pace III, and B. M. Oliver

Date Published: February 1995

Prepared for the
U.S. Department of Energy
Office of Basic Energy Sciences
KC 02 01 04 0

Prepared by the
OAK RIDGE NATIONAL LABORATORY
Oak Ridge, Tennessee 37831
managed by
MARTIN MARIETTA ENERGY SYSTEMS, INC.
for the
U.S. DEPARTMENT OF ENERGY
under contract DE-AC05-84OR21400

CONTENTS

LIST OF FIGURES

LIST OF TABLES

Neutron Dosimetry of the HFIR Hydraulic Facility*

S. T. Mahmood†, S. Mirzadeh, K. Farrell,
J. V. Pace III, and B. M. Oliver‡

ABSTRACT

The total, fast, and thermal neutron fluxes at five axial positions in the High Flux Isotope Reactor (HFIR) hydraulic tube have been measured using bare and/or cadmium-covered activation, fission, and helium accumulation flux monitors. The spectrum-averaged, one-group cross sections over selected energy ranges for the reactions used in the measurements were obtained using cross sections from the ENDF/B-V file, and the target region volume-integrated spectrum was calculated with DORT, a two-dimensional discrete ordinates radiation transport code. The fluxes obtained from various monitors are in good agreement. The total and fast (>1 MeV) neutron fluxes vary from 1.6×10^{19} n/m^2·s and 1.6×10^{18} n/m^2·s, respectively, at the ends (HT-1 and -9) of the facility to 4.0×10^{19} n/m^2·s and 4.6×10^{18} n/m^2·s, respectively, at the center (HT-5) of the facility. The thermal-to-fast (> 1 MeV) flux ratio varies from about 5.4 at the center to about 6.7 at the ends of the facility. The ratio of fast flux greater than 0.1 MeV to that greater than 1 MeV is 2.0 and stays almost constant along the length of the tube.

1. INTRODUCTION

The Oak Ridge National Laboratory (ORNL) High Flux Isotope Reactor (HFIR) is a compact, flux trap-type reactor with the capability and facilities for performing a wide variety of irradiations. The trap at the center of the cylindrical core of the HFIR is filled by

*Research supported by the Division of Materials Science, U.S. Department of Energy under contract DE-AC05-840R21400 with Martin Marietta Energy Systems, Inc. One of the authors (S. T. Mahmood) was supported by an appointment to the Oak Ridge National Laboratory Postdoctoral Research Program administered by the Oak Ridge Institute for Science and Education.

†Present address: General Electric Company, Vallecitos Nuclear Center, Pleasanton, CA 94566.

‡Rockwell International, Canoga Park, CA 91309.

a bundle of aluminum target tubes that hold curium-base materials for production of transuranic elements. These tubes are normally accessible only during fuel changes. A single tube, known as the hydraulic tube facility, passes completely through the bundle and exits the reactor. It conducts a train of small capsules, or rabbits, in and out of the core on demand. The train is driven by hydraulic pressure. The hydraulic tube is in constant use for a variety of purposes, principally for production of isotopes for medical applications.

The neutron fluxes in the trap are not only very high, about 10^{19} n/m^2·s, they are steady during most of the 21-d fuel cycle, and they are reproduced from one cycle to another. The neutron fluxes along the length of the rabbit train were measured carefully about 20 years ago,[1,2] and those data have provided a basis from which a required neutron exposure at any level in the train can be achieved by control of exposure time alone. However, some changes have been implemented in the trap region since the late 1980s. The reactor operating power has been reduced from 100 to 85 MW, and the hydraulic tube which formally occupied the central position in the target bundle has been moved to a different position. Transuranium production is now more stringent and many of the target positions are occupied by a materials irradiation facility and by aluminum dummy targets. These changes will have altered the availability of neutrons in the trap. Consequently, the fluxes in the hydraulic tube need to be redetermined. A reliable flux and spectrum profile is needed, also, to support a new program of radiation embrittlement studies of ferritic steels utilizing the hydraulic tube facility. Accordingly, we have performed comprehensive neutron dosimetry of the hydraulic tube facility using refined activation techniques, cross section data bases, and calculational methods.

2. EXPERIMENTAL DETAILS

2.1 IRRADIATION FACILITY

The irradiations were performed in the HFIR hydraulic tube which is located in position B3 of the target region as shown in Fig. 1. This irradiation facility accommodates nine rabbit capsules, one on top of the other, in a 500-mm stack with position HT-1 at the bottom, level with the bottom of the reactor core, and HT-9 at the top, corresponding to the top of the core. The vertical center of the HT-5 position coincides with the horizontal center line of the core. Loading and unloading of the capsules during reactor operation is carried out by controlling the direction of flow of the cooling water through the tube. The

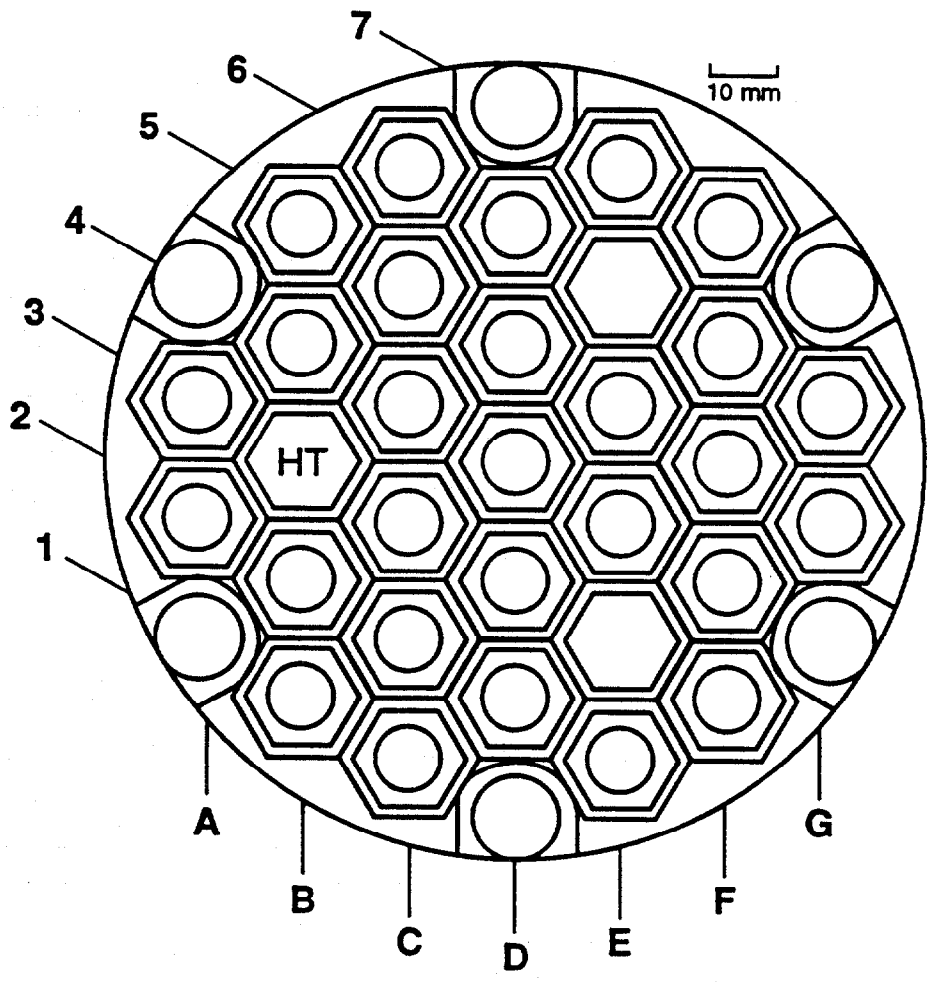

Fig. 1. The central target region of the High Flux Isotope Reactor. The hydraulic tube is located in position B3.

capsules can be either standard finned aluminum cans that are completely sealed or perforated capsules to allow water cooling of the specimens inside.

2.2 IRRADIATION CAPSULES

The capsule material and design used for irradiating the flux monitors were the same as the standard capsule used by the Nuclear Medicine Group in their routine irradiations in the hydraulic tube. The capsules were made according to the drawing shown in Fig. 2, using finned tubing of 6061 aluminum. The ends of the capsules were sealed by welding in end plugs. One end of each capsule was sealed before loading the monitors while the other end was sealed afterwards. Some monitors were shielded with cadmium vials to block out thermal neutrons. Unshielded, or bare, monitors were wrapped in aluminum foil and were loaded at the center of each capsule using aluminum foil spacers at each end. Capsules that contained both bare and Cd-covered monitors had three spacers, one at each end and one in between the bare and Cd-covered monitors.

2.3 SELECTION OF MONITORS

In order to cover as much of the neutron energy range as possible, a number of activation, fission, and helium accumulation monitors were selected. The selection of the monitors was determined by purity of the material, natural abundance and activation cross section of the target isotope, half-life and decay scheme of the product nuclide, burn-out and burn-in of the nuclides, material stability in a radiation environment, heat generation and removal characteristics, and reactivity effects.

Table 1 gives a listing of the selected monitor materials, reactions, abundance of the target isotopes, threshold energies for fast monitors, and thermal neutron activation cross sections for thermal flux monitors. The activation monitors used in this experiment can be divided into two categories, fast flux monitors and thermal flux monitors. Wires of Al, Ti, Fe, Ni, and Cu were used as fast flux monitors; Co, Ag, and dilute alloys of Co, Ag, and Au in aluminum were thermal flux monitors. All of these monitors, except pure Ag, were in the form of high-purity wires with diameters ranging from 0.25 to 0.75 mm and lengths varying from 2 to 50 mm; pure Ag was in the form of 0.025-mm-thick foil. The thermal flux monitors, Au, Ag, and Co, were irradiated bare as well as inside Cd filters. The purpose of the cadmium filters was to discriminate epi- and sub-cadmium flux values. The Au-Al, pure Al, Ag-Al, Co-Al, pure Cu, and pure Ti monitors were acquired from Reactor Experiments, Inc., while pure Fe and Ni monitors were obtained from Materials Research Corporation.

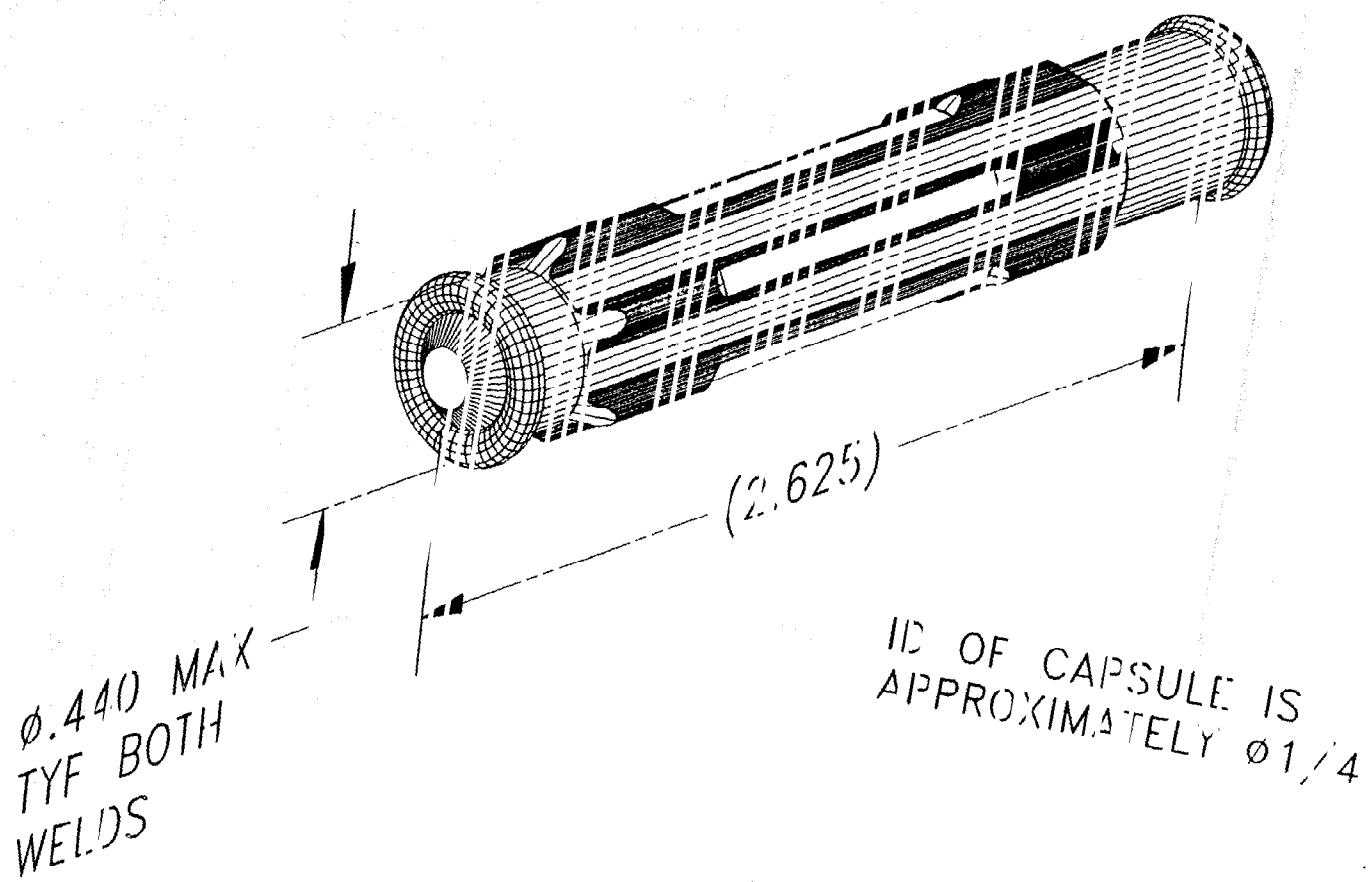

Fig. 2 The finned aluminum capsule used to irradiate the flux monitors (all dimensions are in millimeters).

Table 1. Selected reactions and monitor materials

Reaction	Material	Physical form	Target isotope abundance (%)	Threshold energy (MeV)
$^{27}Al(n, \alpha)^{24}Na$	99.999% Al	0.75-mm-diam wire	100	6.5
$^{46}Ti(n, p)^{46}Sc$	99.793% Ti	0.50-mm-diam wire	7.99	3.8
$^{54}Fe(n, p)^{54}Mn$	99.99% Fe	0.50-mm-diam wire	5.84	2.3
$^{58}Ni(n, p)^{58}Co$	99.951% Ni	0.50-mm-diam wire	67.90	2.1
$^{63}Cu(n, \alpha)^{60}Co$	99.999% Cu	0.75-mm-diam wire	69.17	4.7
$^{237}Np(n, f)^{140}Ba$	$^{237}NpMgO$	sealed in a V capsule	100	0.67
$^{9}Be(n, He)$	99.99% Be	small chunks	100	2.5
				σ_o (barns)
$^{197}Au(n, \gamma)^{198}Au$	0.058% Au-Al	0.25-mm-diam wire	100	98.8
$^{59}Co(n, \gamma)^{60}Co$	0.66% Co-Al 99.514% Co[a]	0.75-mm-diam wire 0.50-mm-diam wire	100	37.45
$^{109}Ag(n, \gamma)^{110m}Ag$	0.145% Ag-Al 99.999% Ag[a]	0.50-mm-diam wire 0.025 mm thick foil	48.65	4.1
$^{6}Li(n, He)$	0.705% Li-Al	0.50-mm-diam wire	7.42	942
$^{10}B(n, He)$	0.502% B-Al	0.50-mm-diam wire	19.58	3838

[a]Used in Cd covers.

In order to provide confirmatory measurements of fast flux from a different type of monitor, conventional fission monitors of ^{237}Np were also included. The Np was in the form of $^{237}NpMgO$ sealed in a small welded vanadium capsule. This was an off-the-shelf monitor from a production batch that has supplied such monitors for many dosimetry experiments including the recent "DOS" series of HFIR pressure-vessel dosimetry experiments.[3,4] Because ^{237}Np has a very high thermal neutron capture cross section, the monitor was encapsulated in a Cd tube with 0.75-mm wall thickness.

Non-activation and non-fission-type dosimeters were also used in this experiment. These are helium accumulation flux monitors (HAFMs) described in American Society for Testing and Materials (ASTM) Standard E910-89 (ref. 5). Neutron absorption in these monitors produces helium, which is a stable reaction product that can be measured with high accuracy. The HAFMs chosen for this experiment were ^{9}Be, ^{6}Li, and ^{10}B. The ^{9}Be is a fast flux monitor. It has several helium-producing reactions, a minor one with a threshold of about 0.7 MeV and a major one with a threshold of 2.5 MeV. This monitor was in the form of small chips. The ^{6}Li and ^{10}B are thermal neutron monitors. These monitors were in the form of 0.5-mm-diam wires of 0.705% Li-Al and 0.502% B-Al. These HAFMs were provided by Rockwell International Corporation from their pedigreed stock.

2.4 IRRADIATION SCHEDULE

In the first set of irradiations (see Table 2), five capsules were prepared with identity marks NM-192 through -196. There were three packages in each capsule. The packages were made by wrapping the monitors in 0.05-mm-thick aluminum foil. The package A in each capsule contained Au-Al and pure Al wires; package B contained Ag-Al, Co-Al, Ni, Fe, Cu, and Ti; package C in capsules NM-192 through -194 contained Al-B, Al-Li, and Be monitors, while package C in capsules NM-195 and -196 contained only Al-B and Al-Li wires. These capsules were irradiated in positions HT-1,-3,-5,-7, and -9 according to the schedule given in Table 2. All capsules were irradiated simultaneously for 1 h at full reactor power of 85 MW.

In the second set, two capsules (NM-197 and -198) were prepared. Each capsule contained bare and cadmium-covered Au, Ag, and Co monitors, and a cadmium-covered Np monitor. The bare Au, Ag, and Co monitors were wrapped in aluminum foil while Cd-covered monitors were in a Cd cylinder with a 1.14-mm-thick and 8.64-mm-high wall and a plug-in cap on the top (ORNL Drawing No. M-12175-CP-939E). The cylinder fitted in the capsule with very small clearance. The Np monitors, sealed in welded vanadium capsules, were inside 0.75-mm-thick cadmium tubing. The capsules NM-197 and -198

Table 2. Irradiation schedule

Capsule	Monitors/filter	HT location	Power (MW)	Irr. time	Date	HFIR irr. #
NM-192	Au,Al,Ag,Co,Ni,Fe, Cu,Ti,B,Li,Be/bare	1	85	1 h	23 Feb., '92	2-92-5[b]
NM-193	"	3	85	1 h	"	2-92-6[b]
NM-194	"	5	85	1 h	"	2-92-7[b]
NM-195	Au,Al,Ag,Co,Ni, Fe,Cu,Ti,B,Li/bare	7	85	1 h		2-92-8[b]
NM-196	"	9	85	1 h	"	2-92-9[b]
NM-197	Au,Ag,Co/ bare & Cd covered + Np/Cd covered	1	10.57	1 h	1 May, '92	4-92-4[c]
NM-198[a]	Au,Ag,Co/ bare & Cd covered + Np/Cd covered	5	10.57	1 h	"	4-92-5[c]
NM-200	Au,Ag,Co/ bare & Cd covered	5	8.85	1 h	21 Nov., '92	10-92-2[d]

[a]Damaged during unloading; only Np monitor was recovered.

[b]HFIR cycle 305.

[c]HFIR cycle 307.

[d]HFIR cycle 313.

were irradiated in positions HT-1 and -5, respectively, for 1 h at a power level of 10.57 MW during startup of the reactor. The reduced power level was used to avoid any excessive heating of the Cd filters. The measured activities were normalized to the full reactor power of 85 MW.

Only the Np monitor was recovered from the NM-198 capsule, the others being inadvertently damaged during unloading of the capsule in the hot cell. Therefore, another capsule, NM-200, was prepared that contained bare and cadmium-covered Au, Ag, and Co monitors. This capsule was irradiated in position HT-5 of the hydraulic tube for 1 h at 8.85 MW. The measured activities of these monitors were also normalized to the full reactor power.

2.5 ACTIVITY MEASUREMENTS ON ACTIVATION AND FISSION MONITORS

Gamma rays emitted by the activation and fission products of the monitors were used to measure the induced activities. Table 3 gives half-lives of the product nuclides and energies and decay fractions of the gamma rays that were counted. A lithium-drifted germanium detector [Ge(Li)], connected to a personal computer-based multichannel analyzer, was used for these measurements. The detector was enclosed in a lead shield, and the source-to-detector distance was maintained at 0.3 m. The system was calibrated according to the ASTM Standard Procedure E 181-82 (1991) [ref. 6] using standard sources traceable to the National Institute of Standards and Technology. The detector efficiency was measured at several gamma energies between 100 and 1600 keV, and a polynomial was fitted to the data to determine efficiency at the desired energies. Periodic quality control checks were made to verify the efficiency and energy calibrations. The counting time for each monitor was varied to obtain total accumulated photopeak counts, in most cases between 10,000 and 20,000. The background counts were also accumulated for the same length of time.

Many fission products are produced in ^{237}Np fission monitors, among which is ^{140}Ba, having a half-life of 12.75 d. Barium-140 emits gamma rays of several energies; however, these are not easily detected in the presence of other fission products. Barium-140 activity was, therefore, indirectly determined by counting gamma rays from its daughter product, ^{140}La, several days after irradiation.

2.6 HELIUM MEASUREMENTS ON HAFMs

The HAFMs were analyzed at Rockwell International. Each piece of the HAFMs Li, Be, and B was carefully weighed and placed in a small, tungsten wire, electrical

Table 3. Activation and fission monitors product nuclide data

Reaction	Half-life	Gamma ray used	
		Eγ (keV)	Decay fraction
$^{27}Al(n, \alpha)^{24}Na$	15.03 h	1368.6	1.0
$^{46}Ti(n, p)^{46}Sc$	83.8 d	889.3	1.0
$^{54}Fe(n, p)^{54}Mn$	312.2 d	835.0	1.0
$^{58}Ni(n, p)^{58}Co$	70.78 d	811.0	0.9944
$^{63}Cu(n, \alpha)^{60}Co$	5.272 y	1173.2	1.0
$^{237}Np(n, f)^{140}Ba$	12.75 d 1.68 d(^{140}La)	1596.0	0.954
$^{197}Au(n, \gamma)^{198}Au$	2.697 d	411.8	0.986
$^{59}Co(n, \gamma)^{60}Co$	5.272 y	1173.2	1.0
$^{109}Ag(n, \gamma)^{110m}Ag$	252.2 d	885.0	0.735

resistance heater in a vacuum chamber attached to a mass spectrometer. After achieving a satisfactory vacuum level, the specimen was rapidly evaporated to release the helium, which was then measured in a mass spectrometer. The system was calibrated against a known volume of helium-3 spiked into the system. The measured helium concentrations were expressed as atomic parts per billion (appb). A full description of the helium analysis of the HAFMs is available in a letter report from Rockwell International Corporation, dated May 20, 1992 (RI ref. 92RC00784).

3. DATA ANALYSIS AND RESULTS

3.1 DETERMINATION OF REACTION RATES

For the activation monitors, the measured gamma counts were converted to the corresponding saturation activities (reaction rates) expressed as disintegrations per second per target isotope, and the activities were corrected for self-shielding, depletion of the target isotope, and burn-in and burn-out of the product nuclide using ASTM Standard Procedures.[7-15] The self-shielding factors were negligible for these monitors except for Cu which required a 5% correction. The burn-up factors for 1 h irradiation were also insignificant except for the nuclide ^{58}Co from the reaction ^{58}Ni (n,p) ^{58}Co and ^{198}Au from the reaction ^{197}Au (n,γ) ^{198}Au. The measured saturation activities for the bare activation monitors from capsules NM-192 to -196 are given in Table 4, while saturation activities for the bare and Cd-covered thermal flux monitors from capsules NM-197 and -200 are given in Table 5. Table 5 also lists the difference of the saturation activities of the bare and Cd-covered monitors and the measured cadmium ratio (R) for each monitor.

When ^{237}Np is irradiated in a neutron field with a high component of thermal flux, most of the ^{140}Ba activity is produced from fission of ^{238}Np which is produced by the reaction ^{237}Np (n,γ) ^{238}Np with thermal neutrons. To minimize this contribution in these irradiations, the fission monitors were enclosed in 0.75-mm-thick Cd filters. Therefore, most of the ^{140}Ba activity induced in these monitors was due to fast neutron fissions in ^{237}Np. There is, however, some contribution from photofissions produced by high-energy gamma rays in the irradiation facility and thermal neutron fission of ^{239}Pu, which is present as an impurity. The measured ^{140}La activities were not corrected for these contributions. The measured ^{140}La activities were converted to the corresponding fission rates using the relation:[16]

Table 4. Saturation activities[a] of the bare activation and helium accumulation monitors and Cd-covered fission monitors

(disintegrations per second per atom of target isotope)

Reaction	HT-1	HT-3	HT-5	HT-7	HT-9
$^{27}Al(n, \alpha)^{24}Na$	1.45×10^{-13}	3.73×10^{-13}	4.28×10^{-13}	3.74×10^{-13}	1.73×10^{-13}
$^{46}Ti(n, p)^{46}Sc$	2.15×10^{-12}	5.94×10^{-12}	6.61×10^{-12}	5.83×10^{-12}	2.50×10^{-12}
$^{54}Fe(n, p)^{54}Mn$	1.62×10^{-11}	4.44×10^{-11}	4.96×10^{-11}	4.29×10^{-11}	1.84×10^{-11}
$^{58}Ni(n, p)^{58}Co$	2.02×10^{-11}	4.78×10^{-11}	5.55×10^{-11}	4.89×10^{-11}	2.19×10^{-11}
$^{63}Cu(n, \alpha)^{60}Co$	1.33×10^{-13}	2.93×10^{-13}	3.35×10^{-13}	2.84×10^{-13}	1.26×10^{-13}
$^{237}Np(n, f)^{140}Ba$[b]	5.04×10^{-10}	-	1.04×10^{-9}	-	-
$^{9}Be(n, He)$[c]	4.69×10^{-11}	1.60×10^{-10}	1.77×10^{-10}	-	-
$^{197}Au(n, \gamma)^{198}Au$	1.25×10^{-7}	2.78×10^{-7}	2.77×10^{-7}	2.84×10^{-7}	1.48×10^{-7}
$^{59}Co(n, \gamma)^{60}Co$	3.27×10^{-8}	5.89×10^{-8}	6.63×10^{-8}	5.69×10^{-8}	3.11×10^{-8}
$^{109}Ag(n, \gamma)^{110m}Ag$	5.75×10^{-9}	1.26×10^{-8}	1.41×10^{-8}	1.21×10^{-8}	5.91×10^{-9}
$^{6}Li(n, He)$[c]	8.69×10^{-7}	1.67×10^{-6}	1.83×10^{-6}	1.55×10^{-6}	8.45×10^{-7}
$^{10}B(n, He)$[c]	3.74×10^{-6}	7.01×10^{-6}	7.77×10^{-6}	6.54×10^{-6}	3.70×10^{-6}

[a]These activities have been corrected for self-shielding, depletion of the target isotope, and burn-out and burn-in of the product nuclide during irradiation.

[b]Number of fissions per second per atom of target isotope, normalized to full power (85 MW) of the reactor.

[c]Number of He atoms produced per second per atom of target isotope.

Table 5. Saturation activities[a] of the bare and Cd-covered thermal flux monitors

(disintegrations per second per atom of target isotope)

Location		Monitor		
		Au	Ag	Co
HT-1	Bare	1.18×10^{-7}	5.92×10^{-9}	3.18×10^{-8}
	Cd	3.49×10^{-8}	1.68×10^{-9}	1.35×10^{-9}
	Bare-Cd	8.31×10^{-8}	4.24×10^{-9}	3.05×10^{-8}
	R	3.38	3.52	23.56
HT-5	Bare	3.08×10^{-7}	1.50×10^{-8}	6.94×10^{-8}
	Cd	8.79×10^{-8}	4.88×10^{-9}	4.58×10^{-9}
	Bare-Cd	2.20×10^{-7}	1.01×10^{-8}	6.48×10^{-8}
	R	3.50	3.07	15.15

[a]These activities have been corrected for self-shielding, depletion of the target isotope, and burn-out and burn-in of the product nuclide during irradiation.

Notes: Activities have been normalized to full power (85 MW).

R is Cadmium ratio. R values for other HT locations were obtained by interpolation and assuming symmetry around HT-5.

$$\text{Fissions/second/target isotope} = \frac{A(\lambda_2 - \lambda_1)}{N\lambda_2 Y_1(e^{-\lambda_1 t_1} - e^{-\lambda_2 t_1})\lambda_1 t_i}, \quad (1)$$

where

A = ^{140}La activity at the time of measurement (dps),
λ_1 = decay constant for $^{140}Ba = 6.29 \times 10^{-7}$ s^{-1},
λ_2 = decay constant for $^{140}La = 4.78 \times 10^{-6}$ s^{-1},
N = number of ^{237}Np atoms in the monitor,
Y_1 = fission yield of $^{140}Ba = 0.05489$,
t_1 = elapsed time between time of counting and irradiation(s),
t_i = irradiation time(s).

The calculated fission rates are given in Table 4.

The measured helium concentrations (appb) in HAFMs were also converted to helium production rates expressed as the number of He atoms produced per second per target isotope. They are listed in Table 4.

3.2 THERMAL FLUX CALCULATIONS

The true thermal flux, assuming a Maxwellian distribution, was calculated using the relation:[9]

$$\phi_{th} = \left(\frac{A_b}{G_{th}\, g\, \sigma_0}\right)\left(\frac{R-1}{R}\right)\left(\sqrt{\frac{4T}{\pi T_0}}\right), \quad (2)$$

where

ϕ_{th} = true thermal flux ($n/m^2.s$),
A_b = saturation activity of bare monitor (dps),
G_{th} = thermal self-shielding factor,
g = non 1/v factor in the thermal region,
σ_0 = thermal neutron activation cross section (m^2),
R = cadmium ratio,
T_0 = 293.6 K,
T = 333.6 K (the temperature in the hydraulic tube is close to 60°C).

This relation was used to calculate thermal neutron flux using the saturation activities of the bare Au, Ag, and Co monitors given in Tables 4 and 5 along with the cadmium ratios for these monitors. Since cadmium-covered monitors were irradiated in HT locations 1 and 5 only, the cadmium ratios for the monitors at position 3 were obtained though interpolation, and those for positions 7 and 9 were obtained assuming symmetry around position 5, i.e., R values for positions 7 and 9 were assumed to be the same as for positions 3 and 1, respectively. The G_{th}, g, and σ_0 values for these monitors are given in Table 6. The calculated thermal flux values are given in Sect. 3.3.

Table 6. Parameters used in thermal flux calculations[9]

	Au	Ag	Co
G_{th}	1.00	0.99	0.99
g	1.0052	1.0062	1.00
σ_0 (barns)	98.8	4.1	37.45

The thermal neutron flux values at the five HT locations under investigation were also obtained from helium accumulation monitors ^{6}Li and ^{10}B by dividing the measured helium production rates by the thermal neutron cross sections of 942 barns and 3838 barns for the reactions ^{6}Li (n,α) ^{3}H and ^{10}B (n,α) ^{7}Li, respectively.[5] The results were corrected for the irradiation temperature using the square root term in Eq. (2). The thermal flux values obtained from these monitors are also given in Sect. 3.3.

3.3 TOTAL AND FAST FLUX CALCULATIONS

The first step in the evaluation of total and fast fluxes from the measured reaction rates was to calculate the spectral-averaged cross sections for the reactions of interest. Therefore, one-neutron-energy-group dosimetry cross sections were produced over selected energy ranges for the monitors used in the measurements. The HFIR two-dimensional (2-D) geometry model[17] was modified to include the aluminum tube bundle in the target region. The 64-group neutron cross sections used in radiation transport calculations were produced from the 99-group Advanced Neutron Source Library.[18]

The neutron flux was calculated with the DORT,[19] a 2-D discrete ordinates radiation transport code, using the 64-group cross sections. The total volume-integrated

the cross sections. The calculated target region volume-integrated spectrum normalized to one fission neutron is given in Table 7 and is plotted in Fig. 3. With the CRES code,[20] the flux was expanded (using flat weighting) from the 64-group structure to the DOSDAM84 (ref. 21) 640-neutron group structure and folded with the predetermined DOSDAM84 dosimetry cross sections. The results were then averaged over the specific energy ranges and reduced to a one-neutron group. The computed cross sections are given in Table 8. The measured reaction rates were divided by the corresponding calculated cross sections to obtain the total and fast fluxes.

In order to evaluate total flux from bare monitor activities, the reaction cross sections were averaged over the entire neutron energy spectrum:

$$\bar{\sigma}_{\text{Total}} = \frac{\int_{\circ}^{\infty} \sigma(E)\phi(E)dE}{\int_{\circ}^{\infty} \sigma(E)dE} . \tag{3}$$

The lower limit in the integrals was set at 10^{-4} eV and the upper limit at 20 MeV. The calculated average cross sections, along with the measured activities of the bare monitors, were used to determine total flux from each of the monitors.

The definition of spectral-averaged cross section was modified to:

$$\bar{\sigma}_{>E_0} = \frac{\int_{\circ}^{\infty} \sigma(E)\phi(E)dE}{\int_{E_0}^{\infty} \phi(E)dE} , \tag{4}$$

to determine fast flux above neutron energy E_0, which was set at 0.1 and 1 MeV for the corresponding fluxes from activities of the bare fast flux monitors.

Since the activities induced in the cadmium-covered Au, Ag, and Co monitors are due to epi-cadmium neutrons only, the epi-cadmium (> 0.5 eV) flux values were determined from the activities of these monitors in combination with the average cross sections calculated by setting lower and upper limits of both integrals at 0.5 eV and 20 MeV, respectively. The sub-cadmium (< 0.5 eV) flux values were determined from differences of the activities of the bare and cadmium-covered monitors along with the average cross sections evaluated in the sub-cadmium range, i.e., with lower and upper limits of both integrals set at 10^{-4} and 0.5 eV, respectively.

Table 7. Sixty-four group HFIR aluminum target region total volume-integrated neutron spectrum normalized to one fission neutron

Group	Top E (MeV)	Spectrum (n·cm/s)	Group	Top E (MeV)	Spectrum (n·cm/s)
1	2.0000E +01	7.53581E-05	33	2.2974E-01	5.13317E-01
2	1.5941E+01	1.01616E-03	34	1.7411E-01	4.47747E-01
3	1.2706E+01	7.57756E-03	35	1.3195E-01	4.30975E-01
4	1.0127E+01	3.43697E-02	36	1.0000E-01	9.21835E-01
5	8.0722E+00	1.04587E-01	37	4.9224E-02	7.96638E-01
6	6.4340E+00	1.41115E-01	38	2.4230E-02	7.30532E-01
7	5.5234E+00	2.20078E-01	39	1.2017E-02	6.90887E-01
8	4.7417E+00	3.02087E-01	40	6.0042E-03	6.76460E-01
9	4.0707E+00	3.67954E-01	41	3.0000E-03	6.54129E-01
10	3.4946E+00	4.71502E-01	42	1.5220E-03	6.49369E-01
11	3.0000E+00	3.46830E-01	43	7.7217E-04	6.46214E-01
12	2.7235E+00	3.82847E-01	44	3.9110E-04	6.42848E-01
13	2.4725E+00	4.19737E-01	45	1.9776E-04	6.37196E-01
14	2.2447E+00	3.92363E-01	46	1.0000E-04	4.45887E-01
15	2.0378E+00	3.98497E-01	47	6.1780E-05	4.37630E-01
16	1.8500E+00	2.50196E-01	48	3.8168E-05	4.12505E-01
17	1.7497E+00	2.42818E-01	49	2.4082E-05	3.86961E-01
18	1.6548E+00	2.40055E-01	50	1.5518E-05	3.83647E-01
19	1.5651E+00	2.41739E-01	51	1.0000E-05	4.11880E-01
20	1.4803E+00	2.41814E-01	52	6.1780E-06	6.21981E-01
21	1.4000E+00	3.71844E-01	53	3.0000E-06	4.73766E-01
22	1.2816E+00	3.68101E-01	54	1.7700E-06	1.41791E-01
23	1.1732E+00	3.51047E-01	55	3.9700E-07	1.87787E-01
24	1.0740E+00	3.10802E-01	56	3.3000E-07	2.19794E-01
25	9.8315E-01	3.20109E-01	57	2.7000E-07	3.22537E-01
26	9.0000E-01	6.20893E-01	58	2.1500E-07	6.90217E-01
27	7.6525E-01	6.02982E-01	59	1.6200E-07	2.55123E+00
28	6.5068E-01	5.14038E-01	60	1.0400E-07	8.85592E+00
29	5.5326E-01	4.75971E-01	61	5.0000E-08	6.16908E+00
30	4.7043E-01	3.72404E-01	62	3.0000E-08	6.12899E+00
31	4.0000E-01	6.91834E-01	63	1.0000E-08	9.75097E-01
32	3.0314E-01	6.09022E-01	64	4.4500E-09 1.0000E-10	2.60110E-01

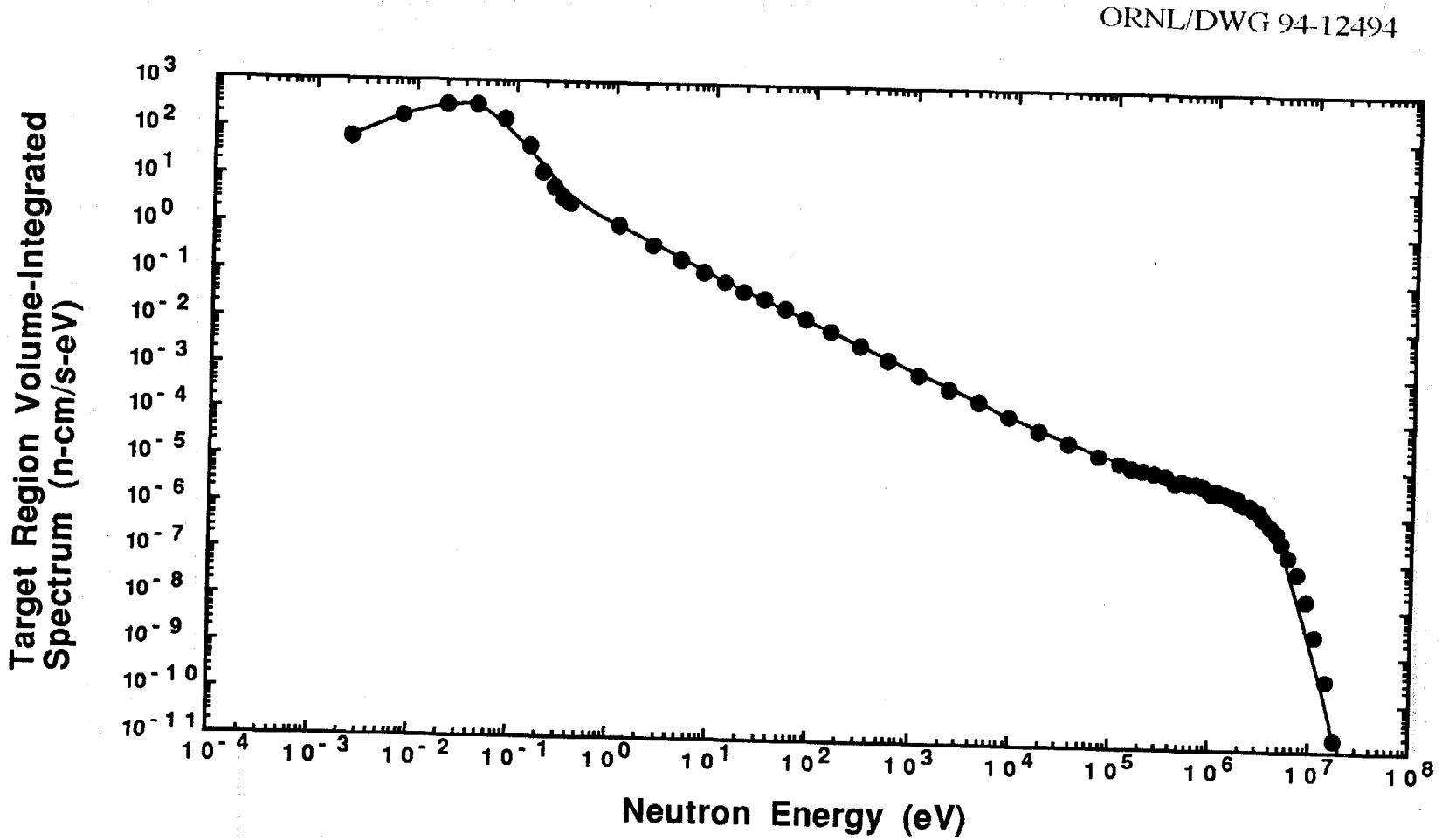

Fig. 3. The calculated target region volume-integrated neutron energy spectrum normalized to one fission neutron.

Table 8. One-group volume-integrated beginning-of-cycle cross sections (reaction or production) averaged over spectrum in the HFIR target region (m^2/neutron · atom)

Reaction	E1=1×10^{-4} eV E2=20.0 MeV E3=1×10^{-4} eV E4=20.0 MeV	E1=1×10^{-4} eV E2=20.0 MeV E3=1.0 MeV E4=20.0 MeV	E1=1×10^{-4} eV E2=20.0 MeV E3=0.1 MeV E4=20.0 MeV	E1=1×10^{-4} eV E2=20.0 MeV E3=0.5 eV E4=20.0 MeV	E1=1×10^{-4} eV E2=20.0 MeV E3=1×10^{-4} eV E4=0.5 eV	E1=0.5 eV E2=20.0 MeV E3=0.5 eV E4=20.0 MeV	E1=1×10^{-4} eV E2=0.5 eV E3=1×10^{-4} eV E4=0.5 eV
^{9}Be(n, He Prod)	4.3284×10^{-30}	3.5328×10^{-29}	1.8404×10^{-29}	9.1540×10^{-30}	-	-	-
^{6}Li(n, He Prod)	4.1424×10^{-26}	3.3810×10^{-25}	1.7613×10^{-25}	-	7.8581×10^{-26}	-	-
^{10}B(n, He Prod)	1.6972×10^{-25}	1.3852×10^{-24}	7.2163×10^{-25}	-	3.2196×10^{-25}	-	-
^{11}B(n, He Prod)	7.0046×10^{-34}	5.7171×10^{-33}	2.9783×10^{-33}	-	-	-	-
^{27}Al(n, α)^{24}Na	1.2055×10^{-32}	9.8393×10^{-32}	5.1256×10^{-32}	2.5459×10^{-32}	-	-	-
^{45}Sc(n, γ)^{46}Sc	1.2017×10^{-27}	9.8082×10^{-27}	5.1095×10^{-27}	-	-	4.7011×10^{-29}	2.2374×10^{-27}
^{46}Ti(n, p)^{46}Sc	1.7182×10^{-31}	1.4024×10^{-30}	7.3055×10^{-31}	3.6338×10^{-31}	-	-	-
^{54}Fe(n, p)^{54}Mn	1.2548×10^{-30}	1.0242×10^{-29}	5.3352×10^{-30}	2.6537×10^{-30}	-	-	-
^{58}Fe(n, γ)^{59}Fe	5.2567×10^{-29}	4.2905×10^{-28}	2.2351×10^{-28}	-	-	5.5519×10^{-30}	9.4739×10^{-29}
^{58}Ni(n, p)^{58}Co	1.6447×10^{-30}	1.3424×10^{-29}	6.9930×10^{-30}	3.4783×10^{-30}	-	-	-
^{59}Co(n, γ)^{60}Co	1.7442×10^{-27}	1.4236×10^{-26}	7.4161×10^{-27}	3.6887×10^{-27}	-	2.6941×10^{-28}	3.0670×10^{-27}
^{63}Cu(n, α)^{60}Co	8.9234×10^{-33}	7.2833×10^{-32}	3.7941×10^{-32}	1.8872×10^{-32}	-	-	-
^{109}Ag(n, γ)^{110m}Ag	3.6666×10^{-28}	2.9927×10^{-27}	1.5590×10^{-27}	7.7543×10^{-28}	-	3.2529×10^{-28}	4.0377×10^{-28}
^{139}La(n, γ)^{140}La	4.1110×10^{-28}	3.3554×10^{-27}	1.7479×10^{-27}	-	-	-	-
^{197}Au(n, γ)^{198}Au	7.2895×10^{-27}	5.9497×10^{-26}	3.0994×10^{-26}	1.5416×10^{-26}	-	6.2806×10^{-27}	8.1944×10^{-27}
^{237}Np(n, f)	2.7159×10^{-29}	2.2167×10^{-28}	1.1548×10^{-28}	5.7437×10^{-29}	-	-	-
^{237}Np(n, γ)^{238}Np	8.5182×10^{-27}	6.9525×10^{-26}	3.6218×10^{-26}	-	-	-	-

Note: Average one-group cross section, $\overline{\sigma} = \frac{\int_{E1}^{E2} \sigma(E)\phi(E)dE}{\int_{E3}^{E4} \phi(E)dE}$, for the integral limits given at the heads of the columns.

The measured total, thermal, fast (E > 0.1 MeV and > 1 MeV), epi-cadmium, and sub-cadmium fluxes are given in Tables 9-13. The average values of these fluxes and some important flux ratios are given in Tables 14 and 15, respectively, and are plotted as a function of HT location in Figs. 4 and 5, respectively.

4. DISCUSSION AND CONCLUSIONS

The purpose of this dosimetry experiment was to measure the neutron flux spectrum along the length of the HFIR hydraulic tube. Out of the nine rabbit capsule positions (HT-1 though -9) in the hydraulic tube, the flux was measured at the five odd-numbered positions using activation, fission, and HAFMs. This measured flux spectrum provides necessary information to analyze the results of the hydraulic tube irradiations that have already been performed and to design future irradiations.

Due to a high thermal neutron component of flux in the hydraulic tube, attempts were made to minimize some undesirable effects of the thermal flux and/or to correct the measurements for these effects that include burn-in and/or burn-out of the product nuclide, self-shielding, depletion of the target isotope, and interference from impurities. Burn-up of the product nuclide in most of the reactions given in Table 1 was negligible except for the nuclides ^{58}Co from the reaction ^{58}Ni (n,p) ^{58}Co and ^{198}Au from the reaction ^{197}Au (n,γ) ^{198}Au. A 1-h irradiation of these monitors in a thermal flux on the order of 10^{19} n/m^2·s required more than 20% correction. The self-shielding factors were also negligible for the monitors used in this experiment, except for Cu which required a 5% correction.

When a ^{237}Np fission monitor is irradiated in a neutron field with a high component of thermal flux, most of the ^{140}Ba activity is produced from the fissioning of ^{238}Np, which is produced by the reaction ^{237}Np (n,γ) ^{238}Np. In addition, ^{239}Pu, which is present as an impurity, also fissions with thermal neutrons and contributes to the ^{140}Ba activity. These contributions in this experiment were minimized by irradiating the fission monitors in 0.75-mm-thick Cd filters. Therefore, most of the ^{140}Ba activity induced in these monitors was due to fast neutron fissions in ^{237}Np. There is, however, always some contribution from ^{238}Np, ^{239}Pu, and photofissions produced by high-energy gamma rays in the irradiation facility. The measured ^{140}La and hence ^{140}Ba activities were not corrected for these contributions due to uncertainties in the magnitude of these effects.

When a ^{9}Be HAFM is exposed to a fast neutron flux, helium is produced though three separate reactions: ^{9}Be (n,α) ^{6}He (α+2n); ^{9}Be (n,2n) ^{8}Be (2α); and ^{9}Be (n,d) 2α.

Table 9. Measured neutron fluxes ($n/m^2 \cdot s$) at HFIR HT-1

Reaction	Total	Thermal	> 0.1 MeV	> 1 MeV
$^{27}Al(n, \alpha)^{24}Na$	1.2×10^{19}		2.8×10^{18}	1.5×10^{18}
$^{46}Ti(n, p)^{46}Sc$	1.3×10^{19}		2.9×10^{18}	1.5×10^{18}
$^{54}Fe(n, p)^{54}Mn$	1.3×10^{19}		3.0×10^{18}	1.6×10^{18}
$^{58}Ni(n, p)^{58}Co$	1.2×10^{19}		2.9×10^{18}	1.5×10^{18}
$^{63}Cu(n, \alpha)^{60}Co$	1.5×10^{19}		3.5×10^{18}	1.8×10^{18}
$^{237}Np(n, f)$	1.9×10^{19}		4.4×10^{18}	2.3×10^{18}
$^{9}Be(n, He)$	1.1×10^{19}		2.6×10^{18}	1.3×10^{18}
$^{197}Au(n, \gamma)^{198}Au$	1.7×10^{19}	1.1×10^{19}		
$^{59}Co(n, \gamma)^{60}Co$	1.9×10^{19}	1.0×10^{19}		
$^{109}Ag(n, \gamma)^{110m}Ag$	1.6×10^{19}	1.2×10^{19}		
$^{6}Li(n, He)$	2.1×10^{19}	1.1×10^{19}		
$^{10}B(n, He)$	2.2×10^{19}	1.1×10^{19}		
			> 0.5 eV	< 0.5 eV
$^{197}Au(n, \gamma)^{198}Au$	1.6×10^{19}	1.0×10^{19}	5.6×10^{18}	1.0×10^{19}
$^{109}Ag(n, \gamma)^{110m}Ag$	1.6×10^{19}	1.2×10^{19}	5.2×10^{18}	1.1×10^{19}
$^{59}Co(n, \gamma)^{60}Co$	1.8×10^{19}	9.9×10^{18}	5.0×10^{18}	1.2×10^{19}

Table 10. Measured neutron fluxes ($n/m^2 \cdot s$) at HFIR HT-3

Reaction	Total	Thermal	> 0.1 MeV	> 1 MeV
$^{27}Al(n, \alpha)^{24}Na$	3.1×10^{19}		7.3×10^{18}	3.8×10^{18}
$^{46}Ti(n, p)^{46}Sc$	3.5×10^{19}		8.1×10^{18}	4.2×10^{18}
$^{54}Fe(n, p)^{54}Mn$	3.5×10^{19}		8.3×10^{18}	4.3×10^{18}
$^{58}Ni(n, p)^{58}Co$	2.9×10^{19}		6.8×10^{18}	3.6×10^{18}
$^{63}Cu(n, \alpha)^{60}Co$	3.3×10^{19}		7.7×10^{18}	4.0×10^{18}
$^{237}Np(n, f)$				
$^{9}Be(n, He)$	3.7×10^{19}		8.7×10^{18}	4.5×10^{18}
$^{197}Au(n, \gamma)^{198}Au$	3.8×10^{19}	2.4×10^{19}		
$^{59}Co(n, \gamma)^{60}Co$	3.4×10^{19}	1.8×10^{19}		
$^{109}Ag(n, \gamma)^{110m}Ag$	3.4×10^{19}	2.6×10^{19}		
$^{6}Li(n, He)$	4.0×10^{19}	2.0×10^{19}		
$^{10}B(n, He)$	4.1×10^{19}	2.2×10^{19}		

Table 11. Measured neutron fluxes ($n/m^2 \cdot s$) at HFIR HT-5

Reaction	Total	Thermal	> 0.1 MeV	> 1 MeV
$^{27}Al(n, \alpha)^{24}Na$	3.5×10^{19}		8.3×10^{18}	4.3×10^{18}
$^{46}Ti(n, p)^{46}Sc$	3.8×10^{19}		9.1×10^{18}	4.7×10^{18}
$^{54}Fe(n, p)^{54}Mn$	3.9×10^{19}		9.3×10^{18}	4.8×10^{18}
$^{58}Ni(n, p)^{58}Co$	3.4×10^{19}		7.9×10^{18}	4.2×10^{18}
$^{63}Cu(n, \alpha)^{60}Co$	3.8×10^{19}		8.8×10^{18}	4.6×10^{18}
$^{237}Np(n, f)$	3.8×10^{19}		9.0×10^{18}	4.7×10^{18}
$^{9}Be(n, He)$	4.1×10^{19}		9.6×10^{18}	5.0×10^{18}
$^{197}Au(n, \gamma)^{198}Au$	3.8×10^{19}	2.4×10^{19}		
$^{59}Co(n, \gamma)^{60}Co$	3.8×10^{19}	2.2×10^{19}		
$^{109}Ag(n, \gamma)^{110m}Ag$	3.9×10^{19}	2.8×10^{19}		
$^{6}Li(n, He)$	4.4×10^{19}	2.3×10^{19}		
$^{10}B(n, He)$	4.6×10^{19}	2.4×10^{19}		
			> 0.5 eV	< 0.5 eV
$^{197}Au(n, \gamma)^{198}Au$	4.3×10^{19}	2.7×10^{19}	1.4×10^{19}	2.7×10^{19}
$^{109}Ag(n, \gamma)^{110m}Ag$	4.1×10^{19}	2.9×10^{19}	1.5×10^{19}	2.5×10^{19}
$^{59}Co(n, \gamma)^{60}Co$	4.0×10^{19}	2.3×10^{19}	1.7×10^{19}	2.1×10^{19}

Table 12. Measured neutron fluxes ($n/m^2 \cdot s$) at HFIR HT-7

Reaction	Total	Thermal	> 0.1 MeV	> 1 MeV
$^{27}Al(n, \alpha)^{24}Na$	3.1×10^{19}		7.3×10^{18}	3.8×10^{18}
$^{46}Ti(n, p)^{46}Sc$	3.4×10^{19}		8.0×10^{18}	4.2×10^{18}
$^{54}Fe(n, p)^{54}Mn$	3.4×10^{19}		8.0×10^{18}	4.2×10^{18}
$^{58}Ni(n, p)^{58}Co$	3.0×10^{19}		7.0×10^{18}	3.7×10^{18}
$^{63}Cu(n, \alpha)^{60}Co$	3.2×10^{19}		7.5×10^{18}	3.9×10^{18}
$^{237}Np(n, f)$				
$^{9}Be(n, He)$				
$^{197}Au(n, \gamma)^{198}Au$	3.9×10^{19}	2.4×10^{19}		
$^{59}Co(n, \gamma)^{60}Co$	3.3×10^{19}	1.8×10^{19}		
$^{109}Ag(n, \gamma)^{110m}Ag$	3.3×10^{19}	2.5×10^{19}		
$^{6}Li(n, He)$	3.7×10^{19}	1.9×10^{19}		
$^{10}B(n, He)$	3.9×10^{19}	2.0×10^{19}		

Table 13. Measured neutron fluxes ($n/m^2 \cdot s$) at HFIR HT-9

Reaction	Total	Thermal	> 0.1 MeV	> 1 MeV
$^{27}Al(n, \alpha)^{24}Na$	1.4×10^{19}		3.4×10^{18}	1.8×10^{18}
$^{46}Ti(n, p)^{46}Sc$	1.5×10^{19}		3.4×10^{18}	1.8×10^{18}
$^{54}Fe(n, p)^{54}Mn$	1.5×10^{19}		3.4×10^{18}	1.8×10^{18}
$^{58}Ni(n, p)^{58}Co$	1.3×10^{19}		3.1×10^{18}	1.6×10^{18}
$^{63}Cu(n, \alpha)^{60}Co$	1.4×10^{19}		3.3×10^{18}	1.7×10^{18}
$^{237}Np(n, f)$				
$^{9}Be(n, He)$				
$^{197}Au(n, \gamma)^{198}Au$	2.0×10^{19}	1.3×10^{19}		
$^{59}Co(n, \gamma)^{60}Co$	1.8×10^{19}	9.7×10^{18}		
$^{109}Ag(n, \gamma)^{110m}Ag$	1.6×10^{19}	1.2×10^{19}		
$^{6}Li(n, He)$	2.0×10^{19}	1.1×10^{19}		
$^{10}B(n, He)$	2.2×10^{19}	1.1×10^{19}		

Table 14. Average values of the measured neutron fluxes ($n/m^2 \cdot s$) in the HFIR hydraulic tube

HT Location	Total	Thermal	< 0.5 eV	> 0.5 eV	> 0.1 MeV	> 1 MeV
HT-1	1.6×10^{19}	1.1×10^{19}	1.1×10^{19}	5.3×10^{18}	3.2×10^{18}	1.6×10^{18}
HT-3	3.5×10^{19}	2.2×10^{19}			7.8×10^{18}	4.1×10^{18}
HT-5	4.0×10^{19}	2.5×10^{19}	2.4×10^{19}	1.5×10^{19}	8.9×10^{18}	4.6×10^{18}
HT-7	3.4×10^{19}	2.1×10^{19}			7.6×10^{18}	4.0×10^{18}
HT-9	1.7×10^{19}	1.1×10^{19}			3.3×10^{18}	1.7×10^{18}

Table 15. Measured flux ratios in the HFIR hydraulic tube

Location	$\phi_{th} / \phi > 1$ MeV	$\phi_{th} / \phi > 0.1$ MeV	$\phi > 0.1$ MeV $/ \phi > 1$ MeV
HT-1	6.88	3.43	2.00
HT-3	5.37	2.82	1.90
HT-5	5.43	2.81	1.93
HT-7	5.25	2.76	1.90
HT-9	6.47	3.33	1.94

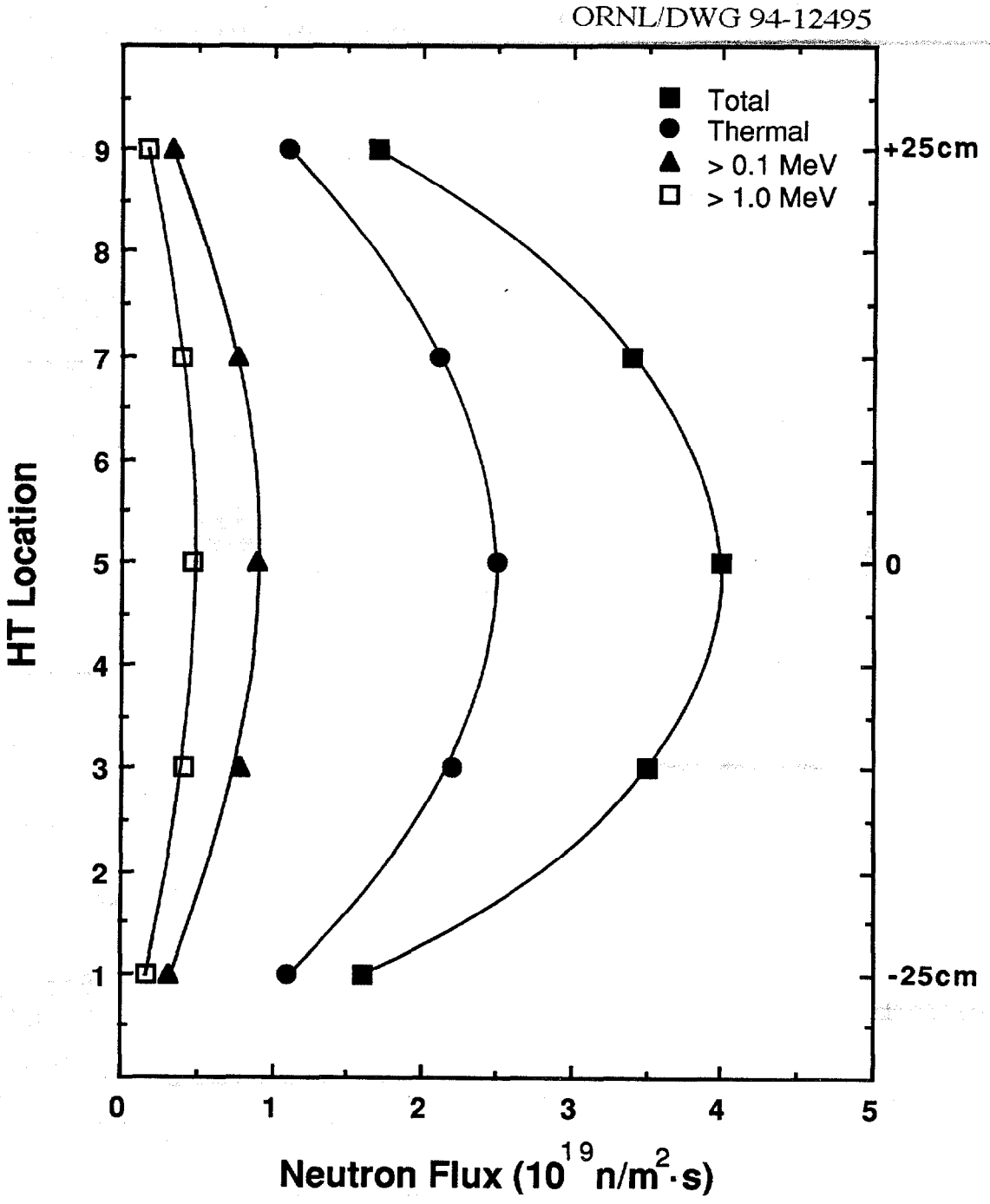

Fig. 4. Measured neutron flux profiles along the length of the hydraulic tube.

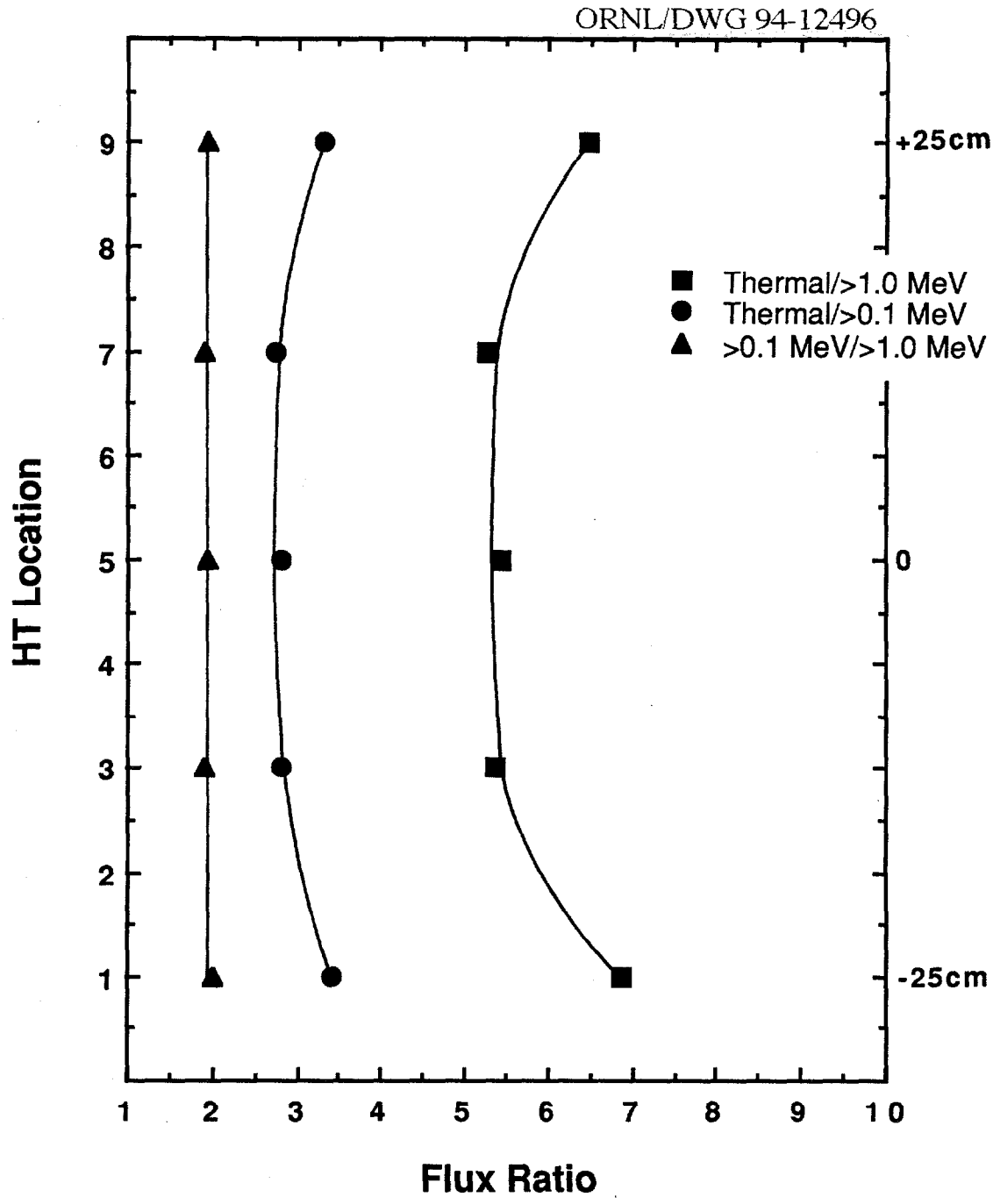

Fig. 5. Some important neutron flux ratios along the length of the hydraulic tube.

Since two alpha particles (helium nuclei) are produced in each reaction, the reaction cross sections in the ENDF-B files have already been multiplied by two and are listed as helium production cross sections that should not be confused with the reaction cross sections. These helium production cross sections were used in combination with the measured helium concentrations to determine total and fast fluxes.

Gamma fields will also create reaction products in fission monitors and in the Be HAFM via (γ,f) and $(\gamma,n)\alpha$ reactions, respectively. However, the threshold energies are high, > 5.4 MeV for ^{237}Np and 1.67 MeV for ^{9}Be, and the reaction cross sections are small, of the order 1/100 and 1/1000 of those for the neutron reactions. Hence, significant contributions from gamma reactions will occur only when the ratio of high-energy gamma rays to high-energy neutrons is high, > 10. Very high ratios exist at the HFIR pressure vessel[4] due to greater attenuation of neutrons than gamma rays in the low-Z beryllium reflector and in the water shield between the core and the vessel, but in the core region, the ratio is close to unity and, hence, the contributions from gamma rays in the hydraulic tube are small for ^{237}Np and negligible for ^{9}Be.

All 12 monitors used in this study yielded very consistent values of the fluxes which, in most cases, are within the expected experimental error. A closer look at total and thermal fluxes measured at five locations shows that in most cases the ^{6}Li and ^{10}B HAFMs yield thermal fluxes that are consistent with those obtained from the other thermal flux monitors, while the total flux values from these two HAFMs are about 40% higher than those obtained from other monitors. Since both of these HAFMs are thermal flux monitors, the helium production cross sections for these monitors are very well established in the thermal neutron energy range, while there are large uncertainties in cross sections at the higher neutron energies. These uncertainties are reflected in the cross section when it is averaged over the entire spectrum, increasing the magnitude of error in the measured fluxes.

The total and fast (> 0.1 MeV and > 1 MeV) fluxes measured using the ^{237}Np fission monitor at location HT-1 of the hydraulic tube are about 13 to 15% higher than those obtained from the other types of monitors. These differences are mainly due to the reasons already mentioned, i.e., contribution from photofissions induced by high-energy photons and thermal neutron fission of ^{239}Pu and ^{238}Np. The measured activities were not corrected for these contributions due to uncertainties in the magnitude of error involved. The total and fast fluxes yielded by the fission monitor at location HT-5 of the hydraulic tube are more consistent with the rest of the monitors mainly due to lower thermal-to-fast flux ratio and the consequent lower gamma-to-neutron flux ratio at that location.

There is a flux peak at the center of the core, as is obvious from the average flux values given in Table 14 and plotted in Fig. 4. The total flux at the top and bottom rabbit positions of the tube is 1.6×10^{19} n/m^2·s, and it increases to 4.0×10^{19} n/m^2·s at the center. The

There is a flux peak at the center of the core, as is obvious from the average flux values given in Table 14 and plotted in Fig. 4. The total flux at the top and bottom rabbit positions of the tube is 1.6 $\times$ 10^{19} n/m^2·s, and it increases to 4.0 $\times$ 10^{19} n/m^2·s at the center. The corresponding values for the thermal flux are 1.1 $\times$ 10^{19} n/m^2·s and 2.5 $\times$ 10^{19} n/m^2·s. As expected, the sub-cadmium flux measured at HT-1 and -5 agrees very well with the thermal flux values. The fast flux (> 0.1 MeV and > 1 MeV) also exhibits the same type of profile, as shown in Fig. 4. Some important flux ratios, given in Table 15, indicate that the thermal-to-fast ratio is a little higher at the ends of the tube as compared to the center, while the ratio of > 0.1 MeV flux to > 1 MeV stays almost constant at two.

The 12 monitors used in this study have their response ranges in different neutron energy intervals, yet they gave very consistent flux values evaluated using the cross sections averaged over the calculated neutron spectrum, indicating that the calculated spectrum is in close agreement with the actual spectrum in the target region, and any spectrum unfolding exercise will not result in very significant improvements. This conclusion is further supported by the results of a recent investigation of some monitor wires in materials experiments in the target region[22] which show that there are no major spectral changes along the active length of the target, and spectrum unfolding results in virtually no adjustment.

Finally, a comparison of the present flux data with earlier data measured in the hydraulic tube[1,2] is given in Table 16. The earlier data were obtained at 100-MW power when the tube was located at the center of the target bundle in the presence of many curium-based targets. The reactor now operates at 85 MW which should reduce the fluxes by 15%. However, the hydraulic tube is now sited closer to the fuel, and the neutron absorption rate in the trap has been altered by the current practice of substituting aluminum components for some of the heavy-element targets. The net effect of these competing factors can be seen in Table 16. The total flux in the hydraulic tube is now reduced by up to 33% and is more symmetrical from the top to the bottom of the tube. The fast fluxes are reduced by up to 25% and are more symmetrical, too. The thermal flux appears to be increased by up to 10% or so.

5. ACKNOWLEDGMENTS

The authors acknowledge C. W. Alexander for helpful discussions and for providing some of the monitors and cadmium filters used in this study.

Table 16. Comparison of the fluxes, $n/m^2 \cdot s$ ($x10^{19}$), in the hydraulic tube with earlier measurements[1,2] made at 100-MW power

Location	Total			E < 0.0253 eV			E > 0.1 MeV			E > 1.0 MeV		
	Ref. 1[a] (100MW)	Ref. 2 (100MW)	Present (85MW)	Ref. 1[a] (100MW)	Ref. 2 (100MW)	Present (85MW)	Ref. 1[a] (100MW)	Ref. 2 (100MW)	Present (85MW)	Ref. 1[a] (100MW)	Ref. 2 (100MW)	Present (85MW)
HT-1	2.4	-	1.6	0.98	1.3	1.1	0.42	0.45	0.32	0.21	-	0.16
HT-3	4.8	-	3.5	1.9	2.1	2.2	0.93	0.97	0.78	0.48	-	0.41
HT-5	5.7	-	4.0	2.3	2.6	2.5	1.1	1.1	0.89	0.56	-	0.46
HT-7	4.2	-	3.4	1.7	2.0	2.1	0.85	0.84	0.76	0.43	-	0.40
HT-9	1.8	-	1.7	0.74	1.0	1.1	0.29	0.37	0.33	0.14	-	0.17

[a] Flux values scaled from those for HT-5 using the measured reaction rates for the other HT locations.

6. REFERENCES

1. F. B. K. Kam and J. H. Swanks, *Neutron Flux Spectrum in the HFIR Target Region,* ORNL-TM-3322, Union Carbide Corp. Nuclear Div., Oak Ridge Natl. Lab., March 1971.

2. K. Farrell to E. E. Bloom, intra-Laboratory correspondence, describing 1974 data measured by F. B. K. Kam, J. H. Swanks, K. Farrell, Oak Ridge Natl. Lab., June 10, 1975.

3. K. Farrell, *et al., The DOS1 Neutron Dosimetry Experiment at the HB-4-A Key 7 Surveillance Site on the HFIR Pressure Vessel,* ORNL/TM-12511, Martin Marietta Energy Systems, Inc., Oak Ridge Natl. Lab., January 1994.

4. I. Remec and F. B. Kam, *Neutron Spectra at Different High Flux Isotope Reactor (HFIR) Pressure Vessel Surveillance Locations*, NUREG/CR-6117, ORNL/TM-12484, Martin Marietta Energy Systems, Inc., Oak Ridge Natl. Lab., December 1993.

5. "Test Method for Application and Analysis of Helium Accumulation Fluence Monitors for Reactor Vessel Surveillance, E 706 (IIIC)," ASTM E 910-89, *1992 Annual Book of ASTM Standards*, Vol. 12.02, American Society for Testing and Materials, New York, 1992.

6. "General Methods for Detector Calibration and Analysis of Radionuclides," ASTM E 181-82 (1991), *1992 Annual Book of ASTM Standards*, Vol. 12.02, American Society for Testing and Materials, New York, 1992.

7. "Terminology Relating to Radiation Measurements and Dosimetry," ASTM E 170-92, *1992 Annual Book of ASTM Standards,* Vol. 12.02, American Society for Testing and Materials, New York, 1992.

8. "Practice for Determining Neutron Fluence Rate, Fluence, and Spectra by Radioactivation Techniques," ASTM E 261-90, *1992 Annual Book of ASTM Standards,* Vol. 12.02, American Society for Testing and Materials, New York, 1992.

9. "Method for determining Thermal Neutron Reaction and Fluence Rates by Radioactivation Techniques," ASTM E 262-86 (1991), *1992 Annual Book of ASTM Standards,* Vol. 12.02, American Society for Testing and Materials, New York, 1992.

10. "Test Method for Measuring Fast Neutron Reaction Rates by Radioactivation of Iron," ASTM E 263-88, *1992 Annual Book of ASTM Standards,* Vol. 12.02, American Society for Testing and Materials, New York, 1992.

11. "Test Method for Measuring Fast Neutron Reaction Rates by Radioactivation of Nickel," ASTM E 264-87, *1992 Annual Book of ASTM Standards,* Vol. 12.02, American Society for Testing and Materials, New York, 1992.

12. "Test Method for Measuring Fast Neutron Reaction Rates by Radioactivation of Aluminum," ASTM E 266-87, *1992 Annual Book of ASTM Standards,* Vol. 12.02, American Society for Testing and Materials, New York, 1992.

13. "Test Method for Measuring Neutron Fluence Rate by Radioactivation of Cobalt and Silver," ASTM E 481-86 (1991), *1992 Annual Book of ASTM Standards,* Vol. 12.02, American Society for Testing and Materials, New York, 1992.

14. "Test Method for Measuring Fast Neutron Reaction Rates by Radioactivation of Copper," ASTM E 523-87, *1992 Annual Book of ASTM Standards,* Vol. 12.02, American Society for Testing and Materials, New York, 1992.

15. "Test Method for Measuring Fast Neutron Reaction Rates by Radioactivation of Titanium," ASTM E 526-87, *1992 Annual Book of ASTM Standards,* Vol. 12.02, American Society for Testing and Materials, New York, 1992.

16. "Standard Test Method for Measuring Reaction Rates by Analysis of Barium-140 from Fission Dosimeters," ASTM E 393-90, *1992 Annual Book of ASTM Standards,* Vol. 12.02, American Society for Testing and Materials, New York, 1992.

17. W. W. Engle, "RZ Base Case, Shielding Input to the HFIR SAR," EPM.HFIR.91.001, Oak Ridge Natl. Lab., June 1991.

18. W. E. Ford III, *et al., ANSL-V: ENDF/B-V Based Multigroup Cross Section Libraries for Advanced Neutron Source (ANS) Reactor Studies*, ORNL-6618, Martin Marietta Energy Systems, Inc., Oak Ridge Natl. Lab., September 1990.

19. W. A. Rhoades and R. L. Childs, "The DORT Two-Dimensional Discrete Ordinates Transport Code," *Nucl. Sci. Eng.* **99**(1) 88-89 (May 1988).

20. J. V. Pace III, "CRES," Oak Ridge Natl. Lab., unpublished cross section averaging code, 1992.

21. W. L. Zijp, *et al., DOSDAM84 - Multigroup Cross Sections in SAND-II Format for Spectral, Integral, and Damage Analyses,* DLC-131, Radiation Shielding Information Center, Oak Ridge Natl. Lab., 1987.

22. Letter report, L. R. Greenwood, Battelle Northwest Laboratories, to D. J. Alexander, Oak Ridge Natl. Lab., July 2, 1993.

INTERNAL DISTRIBUTION

1-2. Central Research Library
3. Document Reference Section
4-5. Laboratory Records Department
6. Laboratory Records Department, RC
7. ORNL Patent Section
8-10. M&C Records Office
11. C. A. Baldwin
12. P. F. Becher
13. J. A. Chapman
14. R. D. Cheverton
15. R. H. Cooper, Jr.
16. G. L. Copeland
17. W. R. Corwin
18. D. F. Craig
19. F. F. Dyer
20. K. F. Eckerman
21-23. K. Farrell
24. G. F. Flanagan
25. W. A. Gabbard
26. M. L. Grossbeck
27. D. W. Heatherly
28. R. W. Hobbs
29. F. B. K. Kam
30. L. L. Horton
31. T. J. Huxford
32. H. T. Kerr
33. J. R. Keiser
34. E. H. Krieg, Jr.
35-37. S. T. Mahmood
38. L. K. Mansur
39. D. W. McDonald
40. J. G. Merkle
41-42. S. Mirzadeh
43. B. F. Myers, Jr.
44. R. K. Nanstad
45. J. V. Pace, III
46. J. E. Pawel
47. R. E. Pawel
48. L. Robinson
49. D. L. Selby
50. C. S. Sims
51. L. L. Snead
52-53. R. E. Stoller
54. L. J. Turner
55. R. M. Westfall
56. S. J. Zinkle
57. H. W. Foglesong (Consultant)
58. E. L. Menger (Consultant)
59. J. G. Simon (Consultant)
60. K. E. Spear (Consultant)

EXTERNAL DISTRIBUTION

61. ATOMIC ENERGY OF CANADA, LTD., Chalk River Nuclear Laboratories, Chalk River, Ontario, Canada KOJ 1JO

    L. M. Howe

62. BATTELLE NORTHWEST LABORATORIES, Richland, WA 99352

    L. R. Greenwood

63-66. BROOKHAVEN NATIONAL LABORATORY, Materials Department, 76 Cornell, Upton, NY 11973

N. Holden
J. O'Conor
D. Rorer
P. R. Tichler

67. EG&G IDAHO, INC., P.O. Box 1625, Idaho Falls, ID 83415

J. W. Rogers

68. HANFORD ENGINEERING DEVELOPMENT LABORATORY, P. O. Box 1970, Richland, WA 99352

M. L. Hamilton

69. JAPAN ATOMIC ENERGY RESEARCH INSTITUTE, Department of Fuels and Materials Research, Tokai-mura, Ibaraki-ken, 319-11 Japan

70. MATERIALS ENGINEERING ASSOCIATES, 9700B Martin Luther King, Jr., Highway, Lanham, MD 20706

71. NATIONAL INSTITUTE OF STANDARDS AND TECHNOLOGY, Gaithersburg, MD 20899

D. E. McGary

72-76. NRC, RES/Division of Engineering, Washington DC 20555

A. Hiser (MS NS 217C)
S. N. Malik (MS NS 217C)
M. E. Mayfield (MS NS 217C)
C. Z. Serpan (MS NS 217C)
A. Taboda (MS NS 217C)

77. ROCKWELL INTERNATIONAL CORPORATION, Canoga Park, CA 91303

B. M. Oliver

78-79. UNIVERSITY OF CALIFORNIA, Department of Chemical and Nuclear Engineering, Ward Memorial Drive, Santa Barbara, CA 93106

G. E. Lucas
G. R. Odette

80. WESTINGHOUSE SAVANNAH RIVER COMPANY, Savannah River Laboratory, Aiken, SC 29808

M. R. Louthan, Jr.

81. DOE, Division of Magnetic Fusion Energy, Washington, DC 20545

F. W. Wiffen (ER-543, J224/GTN)

82-86. DOE, Division of Materials Sciences, Washington, DC 20545

Y. Chen (ER-131, J321/GTN)
A. L. Dragoo (ER-131, F240/GTN)
R. J. Gottschall (ER-131, J321/GTN)
H. Kerch (ER-131, J321/GTN)
I. L. Thomas (ER-132, J321/GTN)

87. DOE, Office of Fossil Energy, Washington, DC 20545

M. I. Singer (FE-14, B115/GTN)

88. DOE, OAK RIDGE OPERATIONS OFFICE, P.O. Box 2001, Oak Ridge, TN 37831-8600

Office of Assistant Manager for Energy Research and Development

89-90. DOE, OFFICE OF SCIENTIFIC AND TECHNICAL INFORMATION, P.O. Box 62, Oak Ridge, TN 37831

For distribution as shown in DOE/OSTI-4500, Distribution Category UC-404 (Materials)